Journal of Fluids and Structures (1999) **13,** 607–630
Article No.: jfls. 1999.0221, available online at http://www.idealibrary.com on IDEAL

A PSEUDOSPECTRAL σ-TRANSFORMATION MODEL OF 2-D NONLINEAR WAVES

M. J. Chern, A. G. L. Borthwick and R. Eatock Taylor

Department of Engineering Science, University of Oxford, Parks Road, Oxford OX1 3PJ, U.K.

(Received 16 December 1997 and in revised form 9 March 1999)

A pseudospectral matrix-element method is proposed for the analysis of 2-D nonlinear time-domain free-surface flow problems. The Chebyshev expansion technique established by Ku & Hatziavramidis has been used to discretize the σ-transformed governing equations including nonlinear boundary conditions. Simulations of nonoverturning transient waves in fixed and base-excited tanks are presented. The results are compared with first- and second-order analytical solutions for sloshing and standing waves, respectively. Excellent agreement is achieved at low values of wave steepness, with the high accuracy due to the close coupling between points. As the wave steepness increases, the influence of higher-order nonlinear components becomes significant, and is modelled by the present scheme. The solution is extremely stable, with the σ-transformation exactly fitting the free-surface boundary, unlike other schemes which have to use free-surface smoothing.

1. INTRODUCTION

Potential flow models have proved to be extremely important in modelling transient free-surface flow problems, including standing waves in fixed tanks, liquid sloshing in base-excited tanks, earthquake-induced transient free-surface flows, and in the design of large diameter offshore structures where loading is in the inertial regime. Although first- (linear) and second-order potential flow analytical solutions have been derived for simple geometries based on perturbation expansion techniques, free-surface flows are often strongly affected by higher-order components. For example, the "ringing" of large diameter structures in steep waves can cause high transient stresses with significant contributions from third-and higher-order wave components. In such cases, low-order solutions of the nonlinear diffraction problem are insufficient to predict the load-response behaviour of the offshore structure. Extension of the perturbation procedure to higher than second order is very cumbersome, and an alternative numerical modelling strategy seems desirable. Nonlinear time-domain simulation then is an appropriate approach.

In the past, much attention has been paid to modelling transient free-surface potential flows by means of the boundary-element technique [e.g., Lin *et al.* (1984), Dold & Peregrine (1986), Grilli *et al.* (1989), Cao *et al.* (1991), Zhao & Faltinsen (1992), and Tulin *et al.* (1994)]. Other authors have used the finite-difference method [e.g., Telste 1985)], or, more recently, the finite-element method [e.g., Wu & Eatock Taylor (1994)]. All of the foregoing approaches give solutions, but smoothing is often necessary to retain stability of the solution (Longuet-Higgins & Cokelet 1976). An alternative, and extremely promising, approach for modelling nonlinear gravity waves has been developed (Fenton & Rienecker 1982; Dommermuth & Yue 1987; Craig & Sulem 1993; Taylor & Vijfvinkel 1998) using series expansions of the surface elevation and potential, with efficient FFT-based Fourier pseudospectral solvers.

0889–9746/99/050607 + 24 $30.00

In the present paper, a Chebyshev pseudospectral matrix-element method is proposed for the solution of Laplace's equation with nonlinear free-surface boundary conditions. This method leads to accurate, stable solutions without the need for free-surface smoothing. The pseudospectral matrix-element method is implemented on a mapped Cartesian rectangular computational grid, with a σ-coordinate transformation applied in the vertical direction to deal with the transient wave elevation. This scheme therefore permits the modelling of steep, but nonoverturning waves.

Spectral methods have been applied to computational fluid dynamics for many years (Hussaini & Zang 1987). In the last decade, a pseudospectral matrix-element method (PSME) was established by Ku & Hatziavramidis (1985) and Ku *et al.* (1987a, b, 1989). A similar idea was provided by Cortes & Miller (1994) as the spectral-difference method. The latter requires that separate one-dimensional expansions be performed for each relevant axis, and the final form of the expansion is the result of the superposition of the one-dimensional results. Cortes & Miller reported that this sort of method can model steep variations very well.

The present paper describes the application of the pseudospectral matrix-element method to steep transient waves, and is laid out as follows. A pseudospectral matrix-element (PSME) based on the Chebyshev expansion technique is proposed in the next section. Then, the mathematical model for free-surface flow is established, based on potential flow theory. A σ-transformation is introduced to map linearly the governing equation and corresponding boundary conditions onto a stretched grid system. Details of the discretized model are presented, followed by its application to increasingly steep waves in fixed and base-excited rectangular tanks. The results are found to be in excellent agreement with analytical solutions at low values of wave steepness, as would be expected. It should be noted that the σ-transformation is unique and so restricts the wave shape to be non-overturning; this means that the model is unable to simulate breaking or nearly breaking waves. It is, however, able to simulate nonbreaking waves of similar steepness to the maximum encountered by offshore platforms in deep water. With extension to 3-D, the present σ-transformed model could be used to model such extreme waves interacting with large diameter vertical cylinders.

2. THE PSEUDOSPECTRAL MATRIX-ELEMENT METHOD

The pseudospectral matrix-element (PSME) method developed by Ku & Hatziavramidis (1985) and Ku *et al.* (1987a, b, 1989) is adopted here. Consider a smooth function $u(x)$ defined on the domain $x \in [-1, 1]$. Then the Chebyshev expansion of u can be written in matrix notation as

$$\mathbf{u} = \mathbf{T}\,\hat{\mathbf{u}}, \tag{1}$$

where $\mathbf{T}$ is the matrix formed by Chebyshev polynomials and $\hat{\mathbf{u}}$ is a vector of Chebyshev coefficients. At each collocation point, we have

$$u_j = u(x_j) \quad \text{and} \quad T_{jk} = T_k(x_j). \tag{2}$$

The collocation points, x_j, can be represented as

$$x_j = \cos\left(\frac{j\pi}{N}\right), \quad j = 0, 1, 2, \ldots, N. \tag{3}$$

The distribution of selected collocation points is relatively sparse in the central part of the interval $[-1, 1]$ and concentrated at the two ends. If the function to be expanded has

a steep gradient in the central part, then more collocation points must be located within the computational domain.

Orthogonality of the Chebyshev polynomials and the Chebyshev–Gauss–Lobatto (CGL) quadrature formula are utilized to obtain the coefficients of the expansion. The matrix representing the transformation from physical space to Chebyshev transform space is available in a simple form, based on

$$\hat{u}_k = \frac{2}{NC_k} \sum_{j=0}^{N} \frac{1}{C_j} u(x_j) \cos \frac{\pi kj}{N}, \quad k = 0, 1, \ldots, N, \tag{4}$$

where

$$C_j, C_k = \begin{cases} 2, & j, k = 0, N, \\ 1, & 1 \leq j, k \leq N-1. \end{cases} \tag{5}$$

In matrix notation, we have

$$\hat{\mathbf{u}} = \hat{\mathbf{T}}\mathbf{u}, \tag{6}$$

where

$$\hat{T}_{kj} = \frac{2}{NC_kC_j} \cos \frac{\pi kj}{N}. \tag{7}$$

This is clearly the inverse of the matrix $\mathbf{T}$ introduced in equation (1).

Moreover, derivatives of the function u can also be transformed to Chebyshev spectral space. The qth derivative expanded in Chebyshev series can be represented in spectral space in the following form:

$$\frac{\mathrm{d}^q u_j}{\mathrm{d}x^q} = \sum_{k=0}^{N} \hat{u}_k^{(q)} T_k(x_j). \tag{8}$$

The coefficients $\hat{u}_k^{(q)}$ of the derivative expansion can be obtained by a recurrence formula which is a form of trigonometric identity. This is given by

$$C_k \hat{u}_k^{(q)} = \hat{u}_{k+2}^{(q)} + 2(k+1)\hat{u}_{k+1}^{(q-1)}, \tag{9}$$

where (in matrix notation)

$$\hat{\mathbf{u}}^{(\mathbf{q})} = \mathbf{G}^{(\mathbf{q})}\hat{\mathbf{u}}. \tag{10}$$

The matrix $\mathbf{G}^{(\mathbf{q})}$ can be obtained from the formula

$$\mathbf{G}^{(\mathbf{q})} = (\mathbf{G}^{(\mathbf{1})})^q, \tag{11}$$

starting from

$$G_{ij}^{(1)} = \begin{cases} 0 & \text{if } i \geq j \text{ or } i+j \text{ even}, \\ \dfrac{2j}{C_i} & \text{otherwise}. \end{cases} \tag{12}$$

In practice, the derivatives are more conveniently expanded in physical space rather than spectral space. The appropriate form of the Chebyshev expansions of the first derivatives can be obtained using equations (8), (10) and (6). Thus, we have

$$\frac{\mathrm{d}\mathbf{u}}{\mathrm{d}x} = \mathbf{T}\hat{\mathbf{u}}^{(\mathbf{1})} = \mathbf{T}\mathbf{G}^{(\mathbf{1})}\hat{\mathbf{u}} = \mathbf{T}\mathbf{G}^{(\mathbf{1})}\hat{\mathbf{T}}\mathbf{u} = \hat{\mathbf{G}}^{(\mathbf{1})}\mathbf{u}, \tag{13}$$

where

$$\hat{\mathbf{G}}^{(1)} = \mathbf{T}\mathbf{G}^{(1)}\hat{\mathbf{T}}. \tag{14}$$

Using the recurrence formula, the Chebyshev expansions in physical space of the second derivative may similarly be derived as

$$\frac{\mathrm{d}^2\mathbf{u}}{\mathrm{d}x^2} = \hat{\mathbf{G}}^{(2)}\mathbf{u}, \tag{15}$$

where

$$\hat{\mathbf{G}}^{(2)} = \mathbf{T}\mathbf{G}^{(2)}\hat{\mathbf{T}} \tag{16}$$

with

$$\mathbf{G}^{(2)} = \mathbf{G}^{(1)}\mathbf{G}^{(1)}. \tag{17}$$

Higher derivatives may be obtained in a similar manner, i.e.,

$$\frac{\mathrm{d}^{(q)}\mathbf{u}}{\mathrm{d}x^{(q)}} = \hat{\mathbf{G}}^{(q)}\mathbf{u}, \tag{18}$$

where

$$\hat{\mathbf{G}}^{(q)} = \mathbf{T}\mathbf{G}^{(q)}\hat{\mathbf{T}}. \tag{19}$$

Equation (18) has several advantages over equation (8). First, $\hat{\mathbf{G}}^{(q)}$ ($q = 1, 2, \ldots,$) is just a function of the number of collocation points rather than other geometric factors. Hence, $\hat{\mathbf{G}}^{(q)}$ only needs to be evaluated once, even if an iterative solver is used. Secondly, the evaluation of the derivatives in physical space by equation (18) can be computed faster. This is because derivatives expanded in spectral space using equation (8) require the coefficients $\hat{\mathbf{u}}_k^{(q)}$ to be determined from equation (4) using FFTs. As indicated by Street *et al.* (1985), however, the matrix-multiply approach (in Fortran) can be significantly faster than FFTs (in assembly language), when the number of collocation points in any given direction does not exceed approximately 100.

3.1. MATHEMATICAL MODEL OF IRROTATIONAL FREE-SURFACE WAVES IN A TANK

3.1. Governing Equation in Cartesian Coordinates

A 2-D nonlinear wave problem is considered here, as depicted in Figure 1. η is the free-surface elevation above still water level, b is the length of the tank and d is the still water depth. A rectangular Cartesian coordinate system is first employed, with origin at the mean free-surface at the left-hand end of the tank. The fluid in the tank is assumed to be inviscid and irrotational. Therefore, the governing equation of fluid motion is given by Laplace's equation,

$$\frac{\partial^2\phi}{\partial x^2} + \frac{\partial^2\phi}{\partial y^2} = 0, \tag{20}$$

where ϕ is the velocity potential function. The velocity components normal to the fixed boundaries are zero by definition. Hence, we have

$$\frac{\partial\phi}{\partial x} = 0, \quad x = 0, b \tag{21}$$

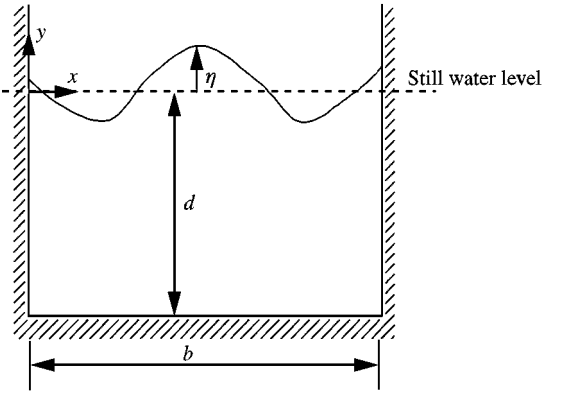

Figure 1. A sketch of the standing wave problem.

and

$$\frac{\partial \phi}{\partial y} = 0, \quad y = -d. \tag{22}$$

The dynamic free-surface boundary condition on $y = \eta$ is

$$\frac{\partial \phi}{\partial t} = -g\eta - \frac{1}{2}\left[\left(\frac{\partial \phi}{\partial x}\right)^2 + \left(\frac{\partial \phi}{\partial y}\right)^2\right]. \tag{23}$$

The kinematic free-surface boundary condition is

$$\frac{\partial \eta}{\partial t} = \frac{\partial \phi}{\partial y} - \frac{\partial \phi}{\partial x}\frac{\partial \eta}{\partial x}. \tag{24}$$

Formulation of the problem is completed by specification of an appropriate initial condition for η.

3.2. Use of the σ-Transformation

A major difficulty in obtaining a numerical solution of the above initial value problem is that at $t > 0$ the coupled nonlinear free-surface conditions, equations (23) and (24), are applied on an unknown line $\eta(x, t)$. In many discretization procedures which have been adopted to deal with this problem, it is necessary to use smoothing to avoid instabilities associated with the propagation of errors in the location of the boundary. Here we attempt to avoid this, by transforming the physical domain onto a rectangular region bounded by horizontal and vertical sides. The approach is to use the so-called σ-transformation, which was originally proposed for meteorological forecasting by Phillips (1957) and has been hitherto applied in the context of oceanic and coastal flows [e.g., Blumberg & Mellor (1980) and Mellor & Blumberg (1985)] and shallow water hydrodynamics [e.g., Stansby & Lloyd (1995)]. $\sigma(x, t)$ is a stretching variable introduced in the vertical direction, taking the value 0 at the seabed and 1 at the free surface.

Figure 2 is a sketch illustrating the σ-transformation. The mapping function $\sigma(x,t)$ is defined as

$$\sigma = \frac{y + d}{h}, \tag{25}$$

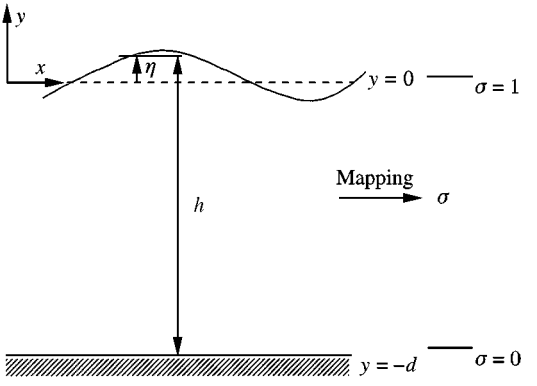

Figure 2. A sketch of the σ-transformation.

where

$$h(x, t) = \eta(x, t) + \mathrm{d}. \tag{26}$$

The derivatives with respect to y and σ are related by

$$\frac{\partial}{\partial y} = \frac{1}{h}\frac{\partial}{\partial \sigma} \quad \text{and} \quad \frac{\partial^2}{\partial y^2} = \frac{1}{h^2}\frac{\partial^2}{\partial \sigma^2}. \tag{27a, b}$$

We need to transform derivatives of the potential function $\phi(x, y, t)$ with respect to x and t into derivatives of $\Phi(x, \sigma, t)$. Using the chain rule, we have

$$\frac{\partial \phi}{\partial t} = \frac{\partial \Phi}{\partial t} + \frac{\partial \Phi}{\partial \sigma}\frac{\partial \sigma}{\partial t} \tag{28a}$$

and

$$\frac{\partial \phi}{\partial x} = \frac{\partial \Phi}{\partial x} + \frac{\partial \Phi}{\partial \sigma}\frac{\partial \sigma}{\partial x}, \tag{28b}$$

where

$$\frac{\partial \sigma}{\partial t} = \frac{\partial}{\partial t}\left(\frac{y + d}{h}\right) = -\frac{\sigma}{h}\frac{\partial \eta}{\partial t} \quad \text{and} \quad \frac{\partial \sigma}{\partial x} = -\frac{\sigma}{h}\frac{\partial \eta}{\partial x}. \tag{29a,b}$$

Therefore, the first derivatives of ϕ with respect to x and t can be rewritten as

$$\frac{\partial \phi}{\partial x} = \frac{\partial \Phi}{\partial x} - \frac{\sigma}{h}\frac{\partial \eta}{\partial x}\frac{\partial \Phi}{\partial \sigma} \tag{30a}$$

and

$$\frac{\partial \phi}{\partial t} = \frac{\partial \Phi}{\partial t} - \frac{\sigma}{h}\frac{\partial \eta}{\partial t}\frac{\partial \Phi}{\partial \sigma}. \tag{30b}$$

The second derivative of $\phi(x, t)$ with respect to x is similarly derived by the chain rule, giving

$$\frac{\partial^2 \phi}{\partial x^2} = \frac{\partial^2 \Phi}{\partial x^2} + \left[2\frac{\sigma}{h^2}\left(\frac{\partial \eta}{\partial x}\right)^2 - \frac{\sigma}{h}\frac{\partial^2 \eta}{\partial x^2}\right]\frac{\partial \Phi}{\partial \sigma} - 2\frac{\sigma}{h}\frac{\partial \eta}{\partial x}\frac{\partial^2 \Phi}{\partial x \partial \sigma} + \left(\frac{\sigma}{h}\frac{\partial \eta}{\partial x}\right)^2 \frac{\partial^2 \Phi}{\partial \sigma^2}. \tag{31}$$

Hence, by using the σ-transformation, we can derive a new governing equation and boundary conditions specified on a rectangular domain. The governing equation is

$$\frac{\partial^2 \Phi}{\partial x^2} + \left[2\,\frac{\sigma}{h^2}\left(\frac{\partial \eta}{\partial x}\right)^2 - \frac{\sigma}{h}\,\frac{\partial^2 \eta}{\partial x^2}\right]\frac{\partial \Phi}{\partial \sigma} - 2\,\frac{\sigma}{h}\,\frac{\partial \eta}{\partial x}\,\frac{\partial^2 \Phi}{\partial \sigma \partial x} + \left[\left(\frac{\sigma}{h}\,\frac{\partial \eta}{\partial x}\right)^2 + \frac{1}{h^2}\right]\frac{\partial^2 \Phi}{\partial \sigma^2} = 0. \tag{32}$$

The dynamic free-surface boundary condition is

$$\frac{\partial \Phi}{\partial t} = \frac{\sigma}{h}\,\frac{\partial \Phi}{\partial \sigma}\,\frac{\partial \eta}{\partial t} - g\eta - \frac{1}{2}\left[\left(\frac{\partial \Phi}{\partial x} - \frac{\sigma}{h}\,\frac{\partial \eta}{\partial x}\,\frac{\partial \Phi}{\partial \sigma}\right)^2 + \left(\frac{1}{h}\,\frac{\partial \Phi}{\partial \sigma}\right)^2\right], \tag{33}$$

and the kinematic free-surface boundary condition is

$$\frac{\partial \eta}{\partial t} = \frac{1}{h}\left[1 + \sigma\left(\frac{\partial \eta}{\partial x}\right)\right]\frac{\partial \Phi}{\partial \sigma} - \frac{\partial \Phi}{\partial x}\,\frac{\partial \eta}{\partial x}, \tag{34}$$

where h is the sum of the water elevation η and the still water depth d.

4. PSEUDOSPECTRAL DISCRETIZATION OF FREE-SURFACE WAVE EQUATIONS

We now use the pseudospectral matrix-element method to solve the initial-boundary value problem in the transformed domain. Accordingly, the governing equation and corresponding boundary conditions are discretized as follows.

We designate N as the number of collocation points in the x-direction, and M as the number in the σ-direction. The computational domain is defined by a further mapping onto $-1 \le X \le 1$, $-1 \le Y \le 1$, using $X = -1 + 2x/b$, $Y = -1 + 2\sigma$. The governing equation for $\Phi_{ij}(1 \le i \le N\text{-}1,\ 1 \le j \le M\text{-}1)$ is

$$\sum_{n=0}^{N} \hat{G}X_{in}^{(2)}\Phi_{nj} + \left[\frac{2(Y_j+1)}{h_i^2}\left(\frac{\partial \eta}{\partial X}\right)_i^2 - \frac{(Y_j+1)}{h_i}\left(\frac{\partial^2 \eta}{\partial X^2}\right)_i\right]\sum_{m=0}^{M} \hat{G}Y_{jm}^{(1)}\Phi_{im} - \frac{(Y_j+1)}{h_i}\left(\frac{\partial \eta}{\partial X}\right)_i \sum_{n=0}^{N}\sum_{m=0}^{M} \hat{G}X_{in}^{(1)}\hat{G}Y_{jm}^{(1)}\Phi_{nm} + \left[\left(\frac{(Y_j+1)}{h_i}\left(\frac{\partial \eta}{\partial X}\right)_i\right)^2 + \frac{b^2}{h_i^2}\right]\sum_{m=0}^{M} \hat{G}Y_{jm}^{(2)}\Phi_{im} = 0. \tag{35}$$

Here we have to deal with derivatives with respect to X and Y. Analogous to $\hat{\mathbf{G}}^{(1)}$ and $\hat{\mathbf{G}}^{(2)}$ in equations (13) and (15) derived for 1-D problems, we use $\hat{\mathbf{G}}\mathbf{X}^{(1)}$, $\hat{\mathbf{G}}\mathbf{Y}^{(1)}$, $\hat{\mathbf{G}}\mathbf{X}^{(2)}$ and $\hat{\mathbf{G}}\mathbf{Y}^{(2)}$ to identify the corresponding terms in 2-D.

Furthermore, the unsteady free-surface boundary equations are discretized using the Adams–Bashforth scheme. When evaluating the dynamic free-surface boundary condition, the pseudospectral method is used to provide an estimate of the right-hand side of equation

(33) at the nth time level as follows:

$$f(\Phi_{i0}^n) = \frac{Y_0 + 1}{h_i}\left(\frac{\partial \eta^n}{\partial t}\right)_i \sum_{m=0}^{M} \hat{G} Y_{0m}^{(1)} \Phi_{im}^n - g\eta_i^n - \frac{1}{2}\left[\left(\frac{2}{b}\sum_{n=0}^{N} \hat{G} X_{in}^{(1)} \Phi_{n0}^n - \frac{2(Y_0 + 1)}{bh_i}\left(\frac{\partial \eta^n}{\partial X}\right)_i \sum_{m=0}^{M} \hat{G} Y_{0m}^{(1)} \Phi_{im}^n\right)^2 + \left(\frac{2}{h_i}\sum_{m=0}^{M} \hat{G} Y_{0m}^{(1)} \Phi_{im}^n\right)^2\right]. \tag{36}$$

Equation (33) is then integrated in time using the Adams–Bashforth method to give

$$\Phi_{i0}^{n+1} = \Phi_{i0}^n + \frac{\Delta t}{12}[23f(\Phi_{i0}^n) - 16f(\Phi_{i0}^{n-1}) + 5f(\Phi_{i0}^{n-2})] + \mathrm{O}(\Delta t^4). \tag{37}$$

Note that the first-order Euler scheme is used to provide information at the first and second time steps, since the Adams–Bashforth is a multistep method.

The kinematic free-surface boundary condition is treated in a similar way. The right hand side of equation (34) is discretized at any time level n using the pseudospectral method to give

$$f(\eta_i^n) = \left[\frac{2}{h_i} + \frac{4(Y_0 + 1)}{b^2 h_i}\left(\frac{\partial \eta^n}{\partial X}\right)_i^2\right] \sum_{m=0}^{M} \hat{G} Y_{0m}^{(1)} \Phi_{im}^n - \frac{4}{b^2}\left(\frac{\partial \eta^n}{\partial X}\right)_i \sum_{n=0}^{N} \hat{G} X_{in}^{(1)} \Phi_{n0}^n. \tag{38}$$

Hence, implementing the Adams–Bashforth method, we obtain

$$\eta_i^{n+1} = \eta_i^n + \frac{\Delta t}{12}[23f(\eta_i^n) - 16f(\eta_i^{n-1}) + 5f(\eta_i^{n-2})] + O(\Delta t^4). \tag{39}$$

The solution proceeds as follows. At each time step, the discretized potential Φ on the free surface is first determined from equations (36) and (37). The spatial derivative $(\partial \eta^n/\partial x)$ is obtained using equation (13) with $\mathbf{u}$ replaced by the vector η^n. Nodal values of η are updated using equations (38) and (39). Equation (38) also provides the required temporal derivative $\partial \eta/\partial t$. Values of Φ throughout the domain are then evaluated by equation (35). The main computational effort at each time step is the solution of equation (35), which is a set of linear algebraic equations for Φ_{ij}. The coefficient matrix is fully populated, and so the matrix equation may be solved by a standard technique such as LU factorization or conjugate gradient methods. Here, we have used the LU factorization method. Unlike other schemes, the σ-transform means that no free-surface smoothing needs to be implemented.

5. NUMERICAL RESULTS

5.1 Standing Wave Motion in a Fixed Rectangular Tank

We specify the following wave elevation as the initial condition:

$$\eta(x, t = 0) = a\cos(2\pi x/b), \tag{40}$$

where a is the amplitude of the initial wave profile, b is the length of the tank and x is the horizontal distance from the left-hand wall. This case is convenient for validation purposes,

because it is simple to obtain the analytical solution when the free-surface condition is linearized. Furthermore, as shown by Wu & Eatock Taylor (1994), expansion of the governing equations by means of the Stokes perturbation procedure also permits one to obtain an analytical solution valid up to second order in wave steepness (defined as a/d where d is the still water depth). We will use this solution to make comparisons with results from the fully nonlinear formulation obtained using the PSME technique. The linear solution for the wave elevation, obtained by separation of variables, is

$$\eta(x, t) = a\cos(\omega_2 t)\cos(k_2 x), \tag{41}$$

and the second-order wave elevation at the centre of the tank, obtained from the perturbation expansions, is

$$\eta_2\left(\frac{b}{2}, t\right) = \frac{1}{8g}\left[2(\omega_2 a)^2\cos 2\omega_2 t + \frac{a^2}{\omega_2^2}(k_2^2 g^2 + \omega_2^4) - \frac{a^2}{\omega_2^2}(k_2^2 g^2 + 3\omega_2^4)\cos\omega_4 t\right]. \tag{42}$$

In equations (41) and (42) the wave number is $k_m = m\pi/b$ for $m = 2$, 4 and

$$\omega_m = [k_m g\tanh(k_m d)]^{1/2}. \tag{43}$$

The results that follow are for a tank having aspect ratio $d/b = 2$. A stretched grid system is established according to the σ-transformation, using equation (25). The physical distribution of the grid points is depicted in Figure 3 (41×21 points). Obviously, the stretched grid system exactly matches the time-dependent free-surface wave profile due to the σ-transformation. To demonstrate that the solution is grid independent, simulations have been performed using different numbers of grid nodes. Time histories of the wave elevation at the centre of the tank, for a steepness $a/d = 0{\cdot}05$, are shown in Figure 4 for 21×11, 41×21 and 61×21 grid points (in the x- and σ-directions, respectively). The figure indicates that 21×11 grid points are sufficient to resolve this nonlinear wave problem. Corresponding results using different nondimensional time steps, $\Delta t^* = \Delta t\sqrt{(g/d)} = 0{\cdot}005$, 0·01, 0·02, are compared in Figure 5. Note that the acceleration due to gravity is selected to be $g = 9{\cdot}8\ \mathrm{m/s^2}$. It may be observed that the results converge, provided the nondimensional time step is no larger than 0·01; hence, this value is adopted in the following simulations. The nondimensional wave period in Figure 5 is about 3·5, and so more than 300 time steps are used in this case to simulate a cycle of the standing wave motion.

In order to validate the proposed scheme, time-dependent free-surface motions at the tank centre for different wave steepness parameters a/d are compared with the corresponding first-order and first-plus-second-order analytical solutions. Figures 6–9 show the growth in high-order nonlinear components with increasing wave steepness (for steepness parameters $a/d = 0{\cdot}005$, 0·03, 0·05 and 0·1). A 41×21 grid is used, except for the steepest waves where the grid is 61×21. The free surface oscillation in Figure 6 for $a/d = 0{\cdot}005$ is in

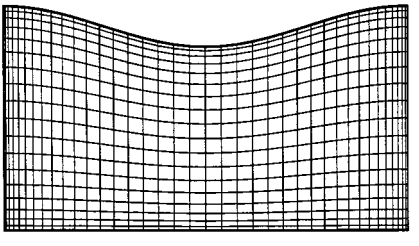

Figure 3. The σ-transformed spectral mesh plotted in the physical domain.

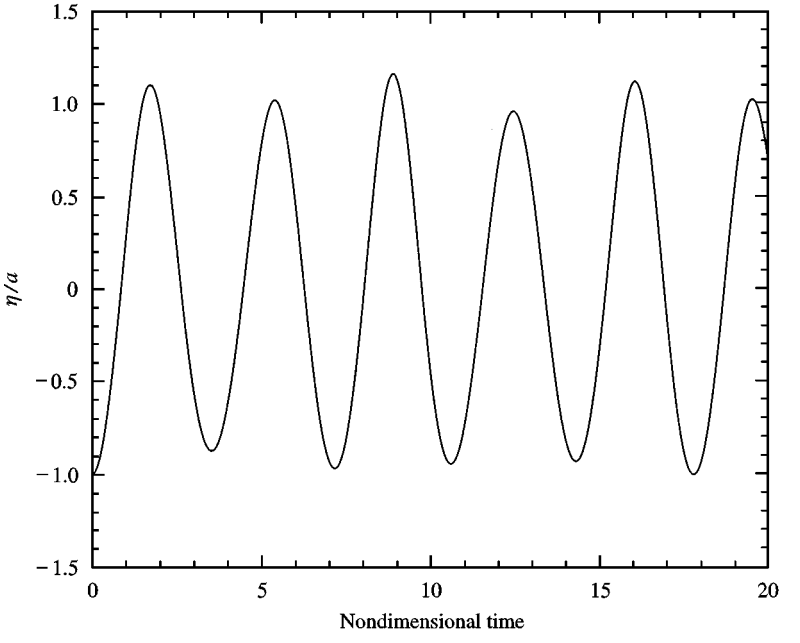

Figure 4. Comparison of solutions using different numbers of collocation points for $a/d = 0{\cdot}05$: —, 21×11; – – –, 41×21; – · – · –, 61×21.

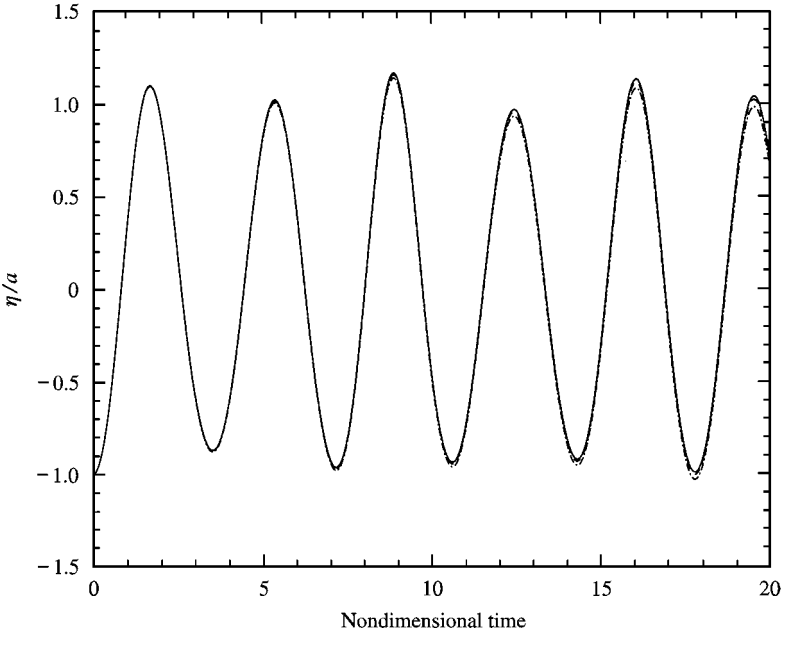

Figure 5. Comparison of solutions using different time steps: —, $\Delta t^* = 0{\cdot}005$; – – –, $\Delta t^* = 0{\cdot}01$; – · – · –, $\Delta t^* = 0{\cdot}02$.

complete agreement with the analytical solution. Nonlinearities gradually become stronger as a/d increases from 0·03 to 0·1 (see Figures 7–9). Although the sum of the first- and second-order solutions is very close to the nonlinear numerical solution in the initial few cycles, it diverges from the analytical solution at later times, as can be seen in Figure 9 for $a/d = 0{\cdot}1$.

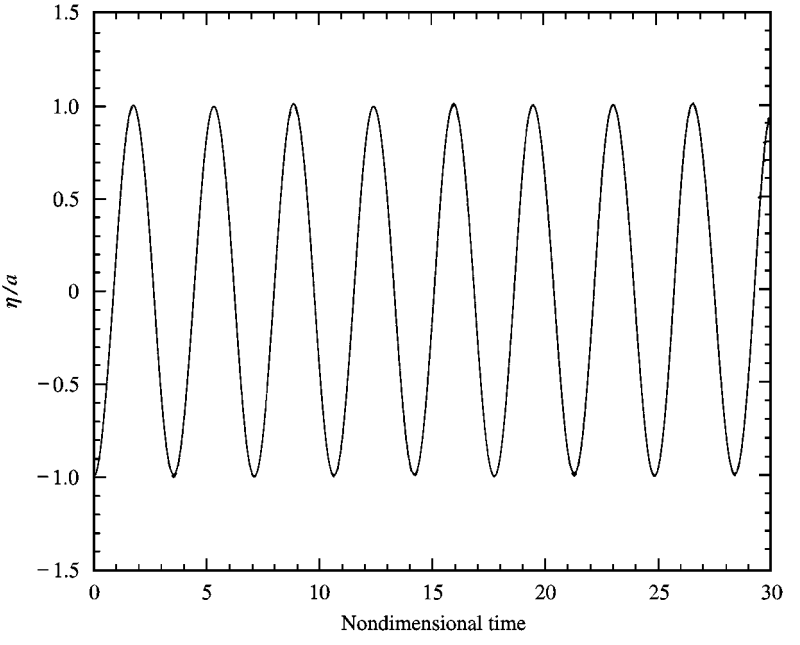

Figure 6. Time history of water elevation at the centre of the tank for $a/d = 0{\cdot}005$: —, numerical solution; – – –, first-order solution; – · – · –, first- and second-order solution.

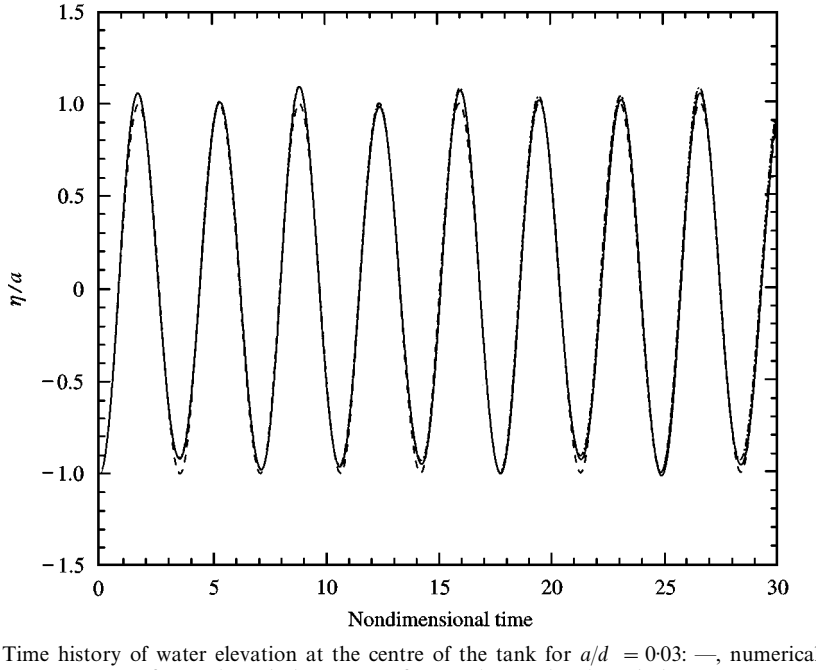

Figure 7. Time history of water elevation at the centre of the tank for $a/d = 0{\cdot}03$: —, numerical solution; – – –, first-order solution; – · – · –, first- and second-order solution.

Wu & Eatock Taylor (1994) observed a similar phenomenon for the same case, using a finite-element model. Owing to the absence of terms above second order, the analytical solutions are incapable of modelling fully the behaviour of steep (and therefore highly nonlinear) free-surface waves.

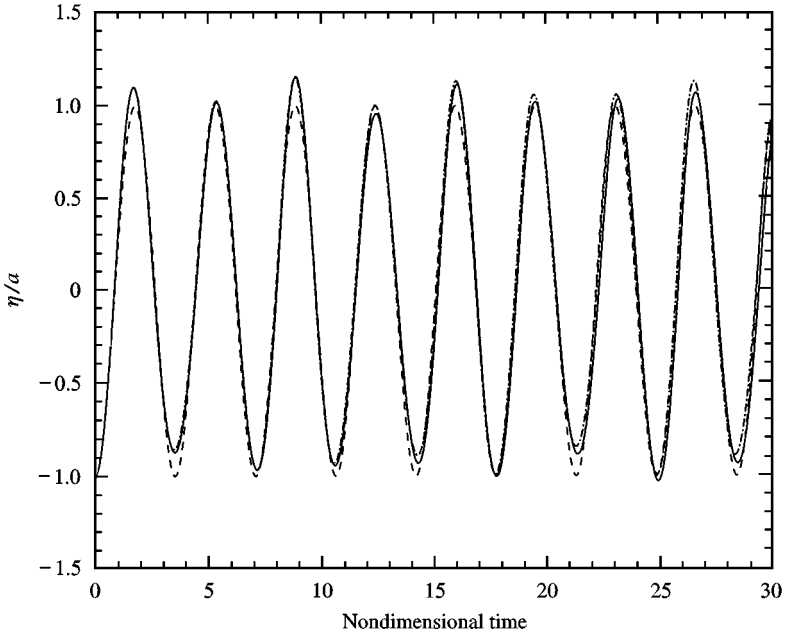

Figure 8. Time history of water elevation at the centre of the tank for $a/d = 0{\cdot}05$. —, numerical solution; - - -, first-order solution; –·–·–, first- and second-order solution.

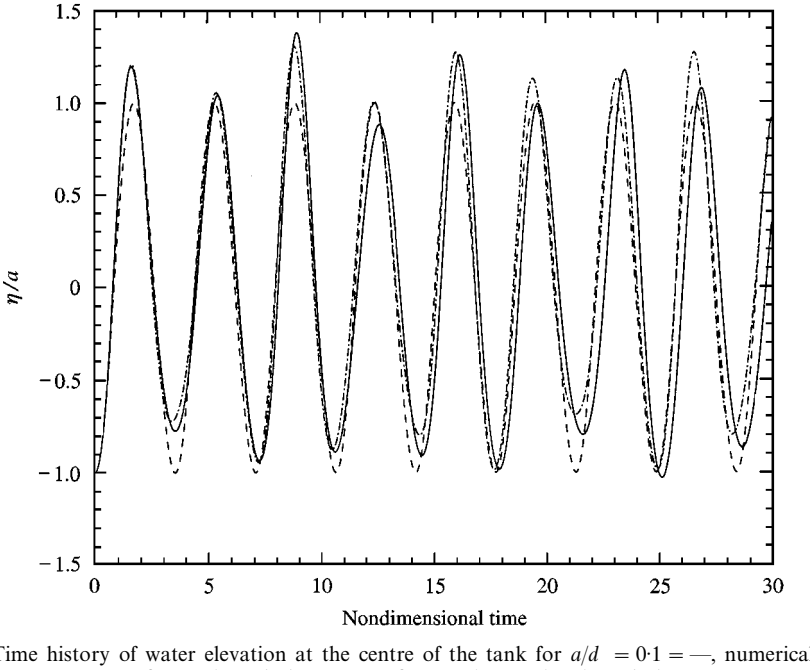

Figure 9 Time history of water elevation at the centre of the tank for $a/d = 0{\cdot}1$ = —, numerical solution; – – –, first-order solution; –·–·–, first- and second-order solution.

Figure 10 superimposes the preceding results for water elevation histories from the pseudospectral model. The profiles reveal that nonlinearity not only changes the peak value but also affects the wave phase.

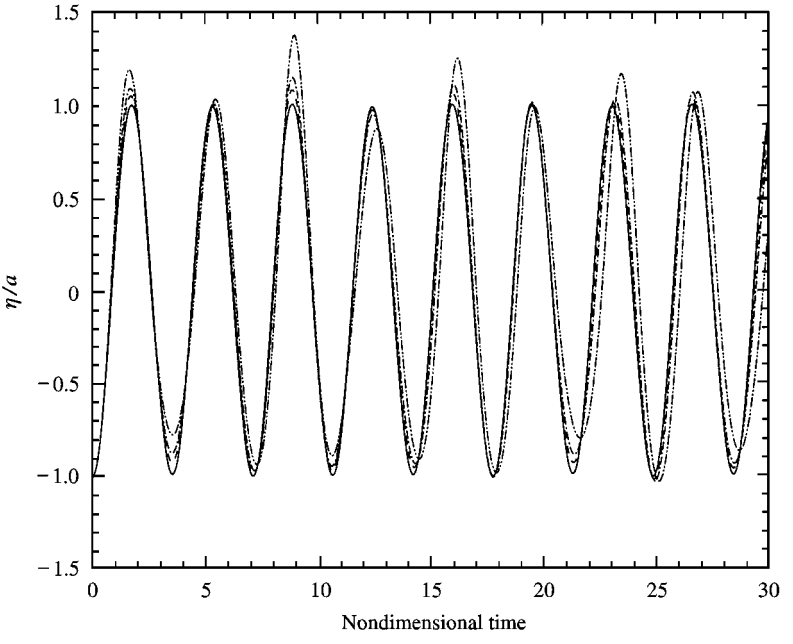

Figure 10 Time history of water elevation at the centre of the tank for different wave steepness conditions: —, $a/d = 0{\cdot}005$; – – –, $a/d = 0{\cdot}03$; – · – · –, $a/d = 0{\cdot}05$; – ·· – ·· –, $a/d = 0{\cdot}1$.

Figures 11–14 present the temporal water surface elevations at the centre and the left wall, again for increasing wave steepness. At $a/d = 0{\cdot}005$, the peaks and troughs of the standing waves are identically opposite to each other with respect to the centre and left-hand end of the tank. As the nonlinearity becomes large, the standing-wave pattern clearly becomes more complicated. There are slight phase differences between the tank centre and wall. Moreover, the amplitudes of troughs and peaks at the two positions are no longer identical.

Figure 15 shows spatial wave profiles at nondimensional times $t = 26$, 27, 28, 29 and 30 for a/d from 0·005 to 0·1. Two nodes are found, as would be expected, for the almost linear waves at $a/d = 0{\cdot}005$ in Figure 15(a). At larger wave amplitudes, the two nodes become less distinct and for $a/d > 0{\cdot}05$ could be said to have disappeared effectively. Even so, it should be noted that these steep wave shapes are still very symmetrical even after 3000 time steps.

Further results are now presented for double-standing waves in the rectangular tank. The initial wave profile is thus given by

$$\eta(x,t=0) = a\cos(4\pi x/b). \tag{44}$$

Four initial wave amplitudes are considered in order to investigate the effect of nonlinearity. Figure 16 shows the free-surface elevation time history of moderately steep waves with $a/d = 0{\cdot}03$, using two grids of 21×11 and 41×21 nodes. The close agreement between the two profiles confirms grid independence; hence, 41×21 grids are used for the four cases considered here. A nondimensional time step, $\Delta t^* = 0{\cdot}01$, is also adopted. For the case shown in Figure 16, there are more than 200 time steps per wave cycle. Figure 17 illustrates water-elevation time histories for $a/d = 0{\cdot}005$, 0·015, 0·025 and 0·03; again, increasing nonlinearity changes the peak and phase of the standing waves. Figure 18 contains spatial

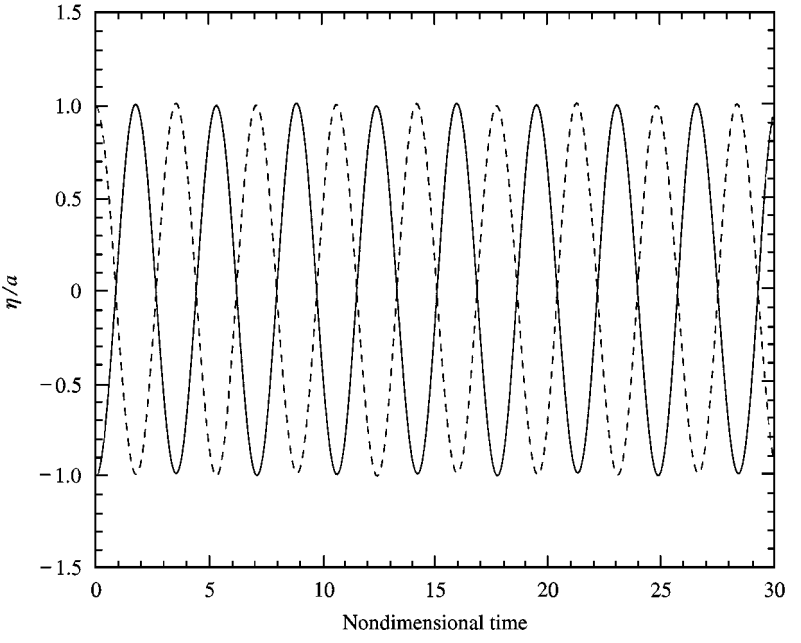

Figure 11. Time history of water elevation at the centre and the wall of the tank for $a/d = 0{\cdot}005$: —, elevation at the centre; - - -, elevation at the wall.

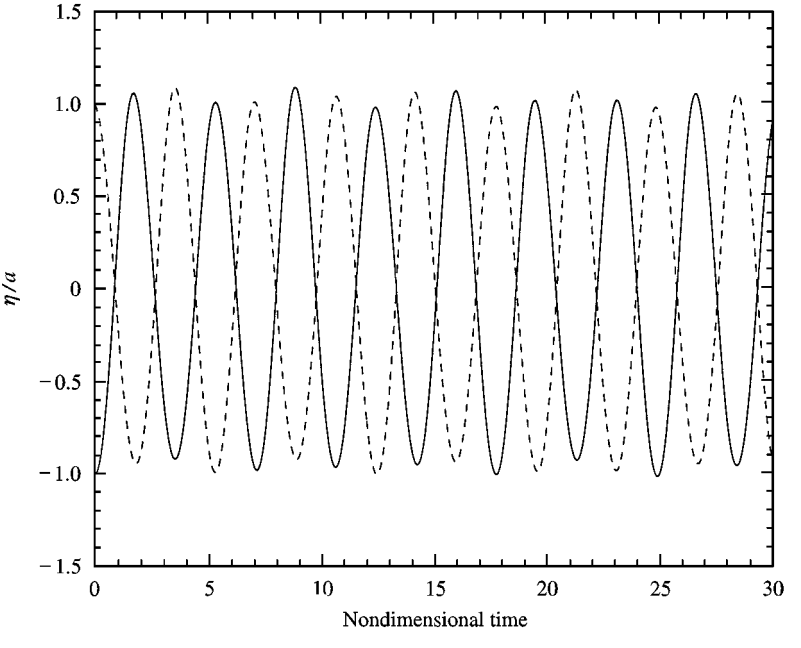

Figure 12. Time history of water elevation at the centre and the wall of the tank for $a/d = 0{\cdot}03$: —, elevation at the centre; - - -, elevation at the wall.

wave profiles at different times throughout the standing wave cycle; in this case, the nondimensional times are $t = 26$, 27, 28, 29 and 30. Again, it is evident that the wave nodes smear with increasing wave nonlinearity.

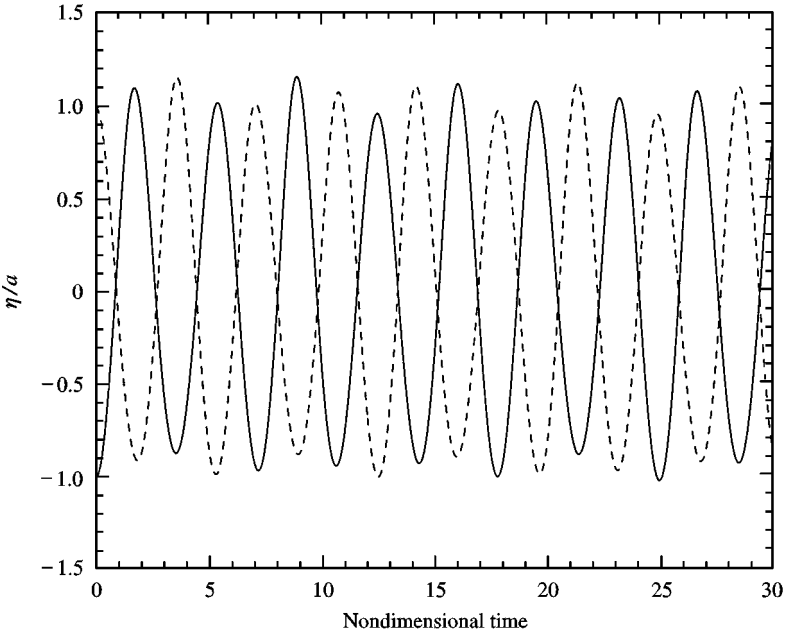

Figure 13. Time history of water elevation at the centre and the wall of the tank for $a/d = 0{\cdot}05$: —, elevation at the centre; - - -, elevation at the wall.

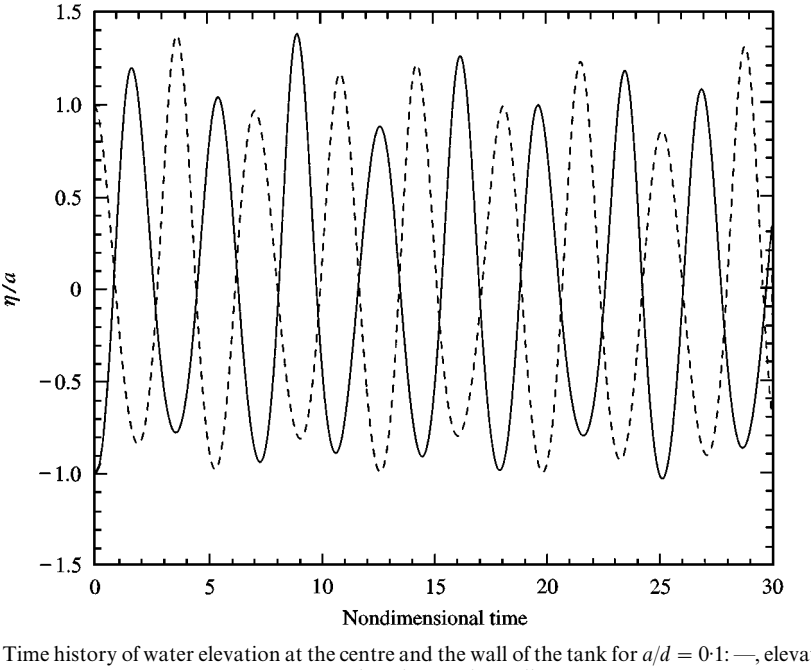

Figure 14. Time history of water elevation at the centre and the wall of the tank for $a/d = 0{\cdot}1$: —, elevation at the centre; - - -, elevation at the wall.

For increasing wavenumbers (i.e., progressively shorter initial wavelengths within the tank), it is reasonable to expect that progressively finer grids and smaller time steps would be required. Even so, it is the authors' experience that the grid parameters are more sensitive to wave steepness than wavenumber for the cases considered above.

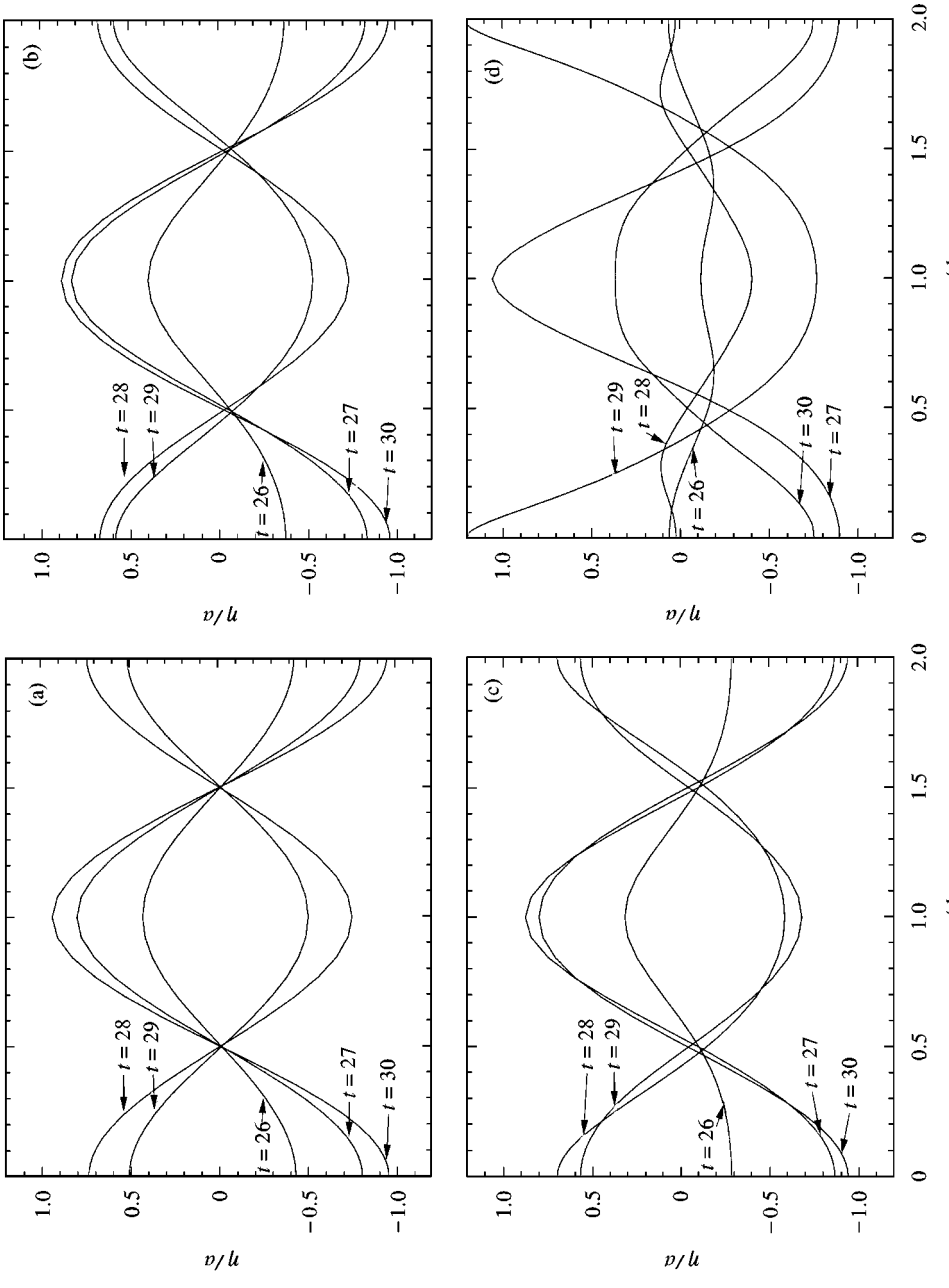

Figure 15. Wave profiles (a) for $a/d = 0{\cdot}005$, (b) for $a/d = 0{\cdot}03$; (c) for $a/d = 0{\cdot}05$; (d) for $a/d = 0{\cdot}1$.

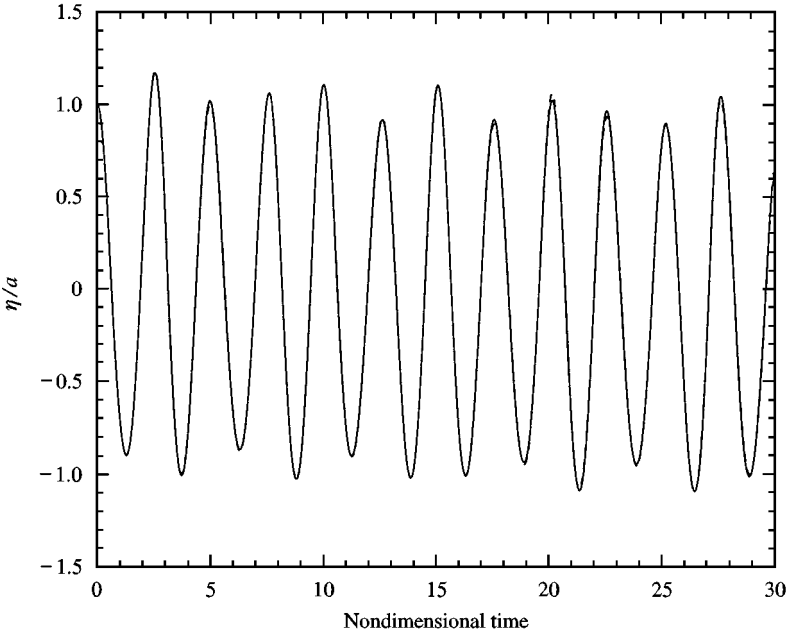

Figure 16. Time history of water elevation at the centre of the tank using different meshes ($a/d = 0{\cdot}03$): —, 21×11; - - -, 41×21.

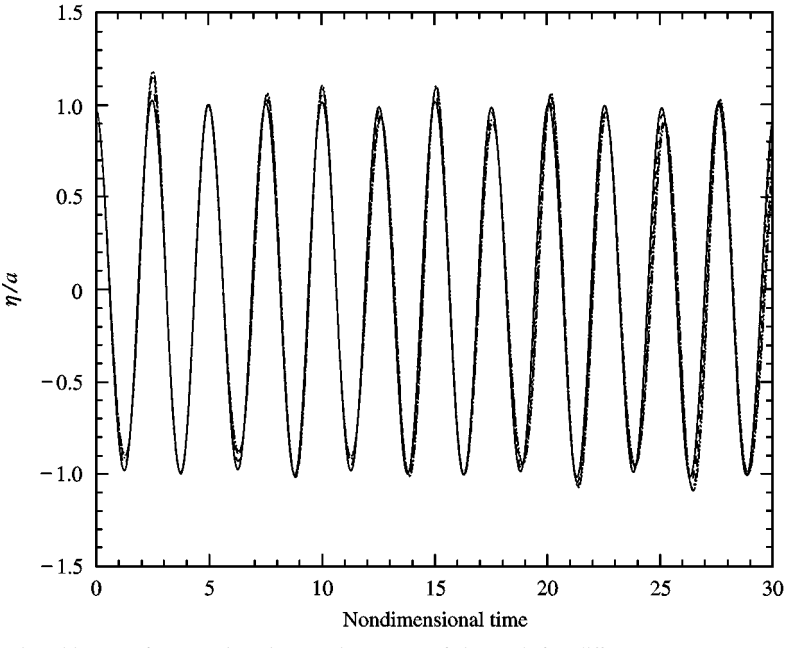

Figure 17. Time history of water elevation at the centre of the tank for different wave steepness conditions: —, $a/d = 0{\cdot}005$; - - -, $a/d = 0{\cdot}015$; - · - · -, $a/d = 0{\cdot}025$; - · · -, $a/d = 0{\cdot}03$.

5.2. Sloshing wave Motion in a Base-excited Rectangular Tank

Dynamic free-surface motions of liquids in tanks are often driven by external forces. Examples include earthquake-excited vibrations or inertia forces due to acceleration of

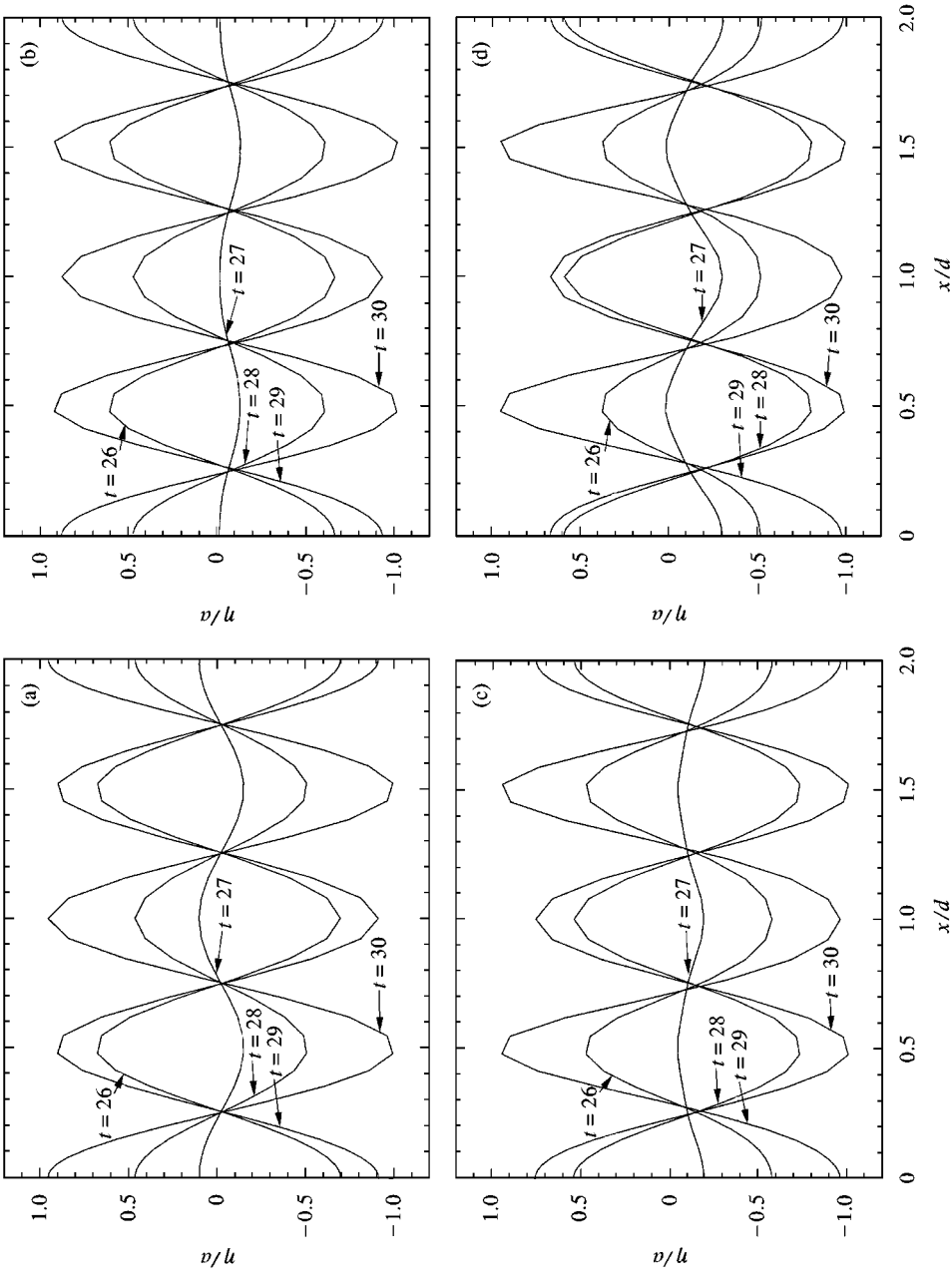

Figure 18. Wave profiles (a) for $a/d = 0{\cdot}005$; (b) for $a/d = 0{\cdot}015$; (c) for $a/d = 0{\cdot}025$; (*d*) for $a/d = 0{\cdot}03$.

a vessel. In the case of a ship, sloshing of liquids within ballast tanks may cause the ship to experience a rolling moment, and even become unstable and capsize. Hence, it is important to predict the effect on ship stability of transient free-surface effects of liquids held in its interior tanks as part of the ship's design procedure. If the forcing frequency is near the natural sloshing frequency, then resonance will occur, resulting in high pressures which may damage the tank walls. Analytical and numerical techniques for predicting sloshing wave motions have been developed over many years. For example, Abramson (1966) used linear theory to analyse small-amplitude sloshing wave motions. Faltinsen (1978), Chen *et al.* (1996) and Wu *et al.* (1998), respectively, used boundary-integral, general coordinate finite difference, and finite-element methods in solving the potential flow problem with nonlinear free-surface boundary conditions. In the foregoing numerical schemes, it was necessary either to introduce artificial damping or to smooth the free surface to prevent numerical instabilities occurring. The availability of alternative theoretical solutions [e.g., Wu *et al.* (1998)] make the case of sloshing free-surface motions in a rectangular tank a suitable validation problem for the present scheme.

Consider a 2-D tank containing liquid, subject to a periodic horizontal base displacement $X_{\text{tank}}(t) = a\sin(\omega t)$, where a is an amplitude, t is time and ω is the angular frequency of the forced motion. The coordinate system is fixed at the centre of the still water free surface, and moves with the tank. The mathematical model for the relative velocity potential will then be the same as equations (20)–(24) except for the dynamical free-surface boundary condition which is written as

$$\frac{\partial \phi}{\partial t} = \frac{\partial \phi}{\partial y}\frac{\partial \eta}{\partial t} - \frac{1}{2}(\nabla\phi\cdot\nabla\phi) - g\,\eta - x\frac{\mathrm{d}^2 X_{\text{tank}}}{\mathrm{d}t^2}, \tag{45}$$

where x and y are measured horizontally and vertically from the centre of the tank, and move with the tank. Wu *et al.* (1998) derive the linear solution for the relative velocity potential to be

$$\phi = a\sum_{n=0}^{\infty}\left(C_n\cos\omega t - \left(C_n + \frac{H_n}{\omega^2}\right)\cos\omega_n t\right)\frac{\cosh k_n(y+\mathrm{d})}{\cosh k_n \mathrm{d}}\sin k_n x, \tag{46}$$

where $k_n = [(2n+1)/b]\pi, \omega_n = (gk_n\tanh k_n\mathrm{d})^{1/2}$, $H_n = \omega^3(4/b)[(-1)^n/k_n^2]$ and $C_n = H_n/(\omega_n^2 - \omega^2)$.

Furthermore, the free-surface elevation can be obtained from

$$\eta = \eta_1 + \eta_2, \tag{47a}$$

where

$$\eta_1 = \frac{a}{g}\left(x\omega^2 + \sum_{n=0}^{\infty} C_n\omega\sin k_n x\right)\sin\omega t \tag{47b}$$

and

$$\eta_2 = -\frac{a}{g}\sum_{n=0}^{\infty}\omega_n\left(C_n + \frac{H_n}{\omega^2}\right)\sin k_n x\sin\omega_n t. \tag{47c}$$

Initial conditions for the velocity potential and free-surface elevation are

$$\phi(x,y,0) = -x\left.\frac{\mathrm{d}X_{\text{tank}}}{\mathrm{d}t}\right|_{t=0} \tag{48}$$

and

$$\eta(x,0) = 0. \tag{49}$$

Wu *et al.* (1998) have explained the physical behaviour of the time-dependent free-surface elevation by considering equation (47a) which contains two terms, each referring to a wave train. The first component, η_1, corresponds to the excitation frequency ω; the second component, η_2, corresponds to the natural frequencies ω_n, and is dominated by ω_0. Higher-order components in η_2 correspond to the higher natural frequencies, and rapidly decay with increasing n. Hence, η is primarily given by the linear sum of waves with frequencies ω and ω_0.

The tank is taken to have an aspect ratio of $d/b = \frac{1}{2}$ where b is its length and d is the still water depth. The first case considered here has nondimensional forcing frequency $\omega/\omega_0 = 0{\cdot}999$ and nondimensional base-displacement amplitude $a/d = 0{\cdot}001$. Figure 19 shows the numerical results and linear analytical solutions for the time-dependent free-surface elevation at the left-hand tank wall, where $x/d = -1$. The amplitude of the free-surface oscillation grows monotonically with time because ω is within 0·1% of the natural frequency ω_0 and so near-resonant conditions apply. The analytical and numerical results are almost identical, except at the peaks and troughs where the numerical model makes increasingly higher predictions due to the growth of nonlinearity with amplitude of the sloshing waves. For the second case, we used $\omega/\omega_0 = 1{\cdot}10$ and $a/d = 0{\cdot}001$. The forcing frequency is now 10% larger than the natural frequency, and a much more complicated surface-elevation time history is obtained at the left-hand wall, as can be seen in Figure 20. Again there is remarkable agreement between the numerical and linear analytical solutions. The linear analysis of Wu *et al.* (1988) predicts the frequency of the wave envelope to be equal to $2\pi/(\omega - \omega_0) = 52{\cdot}25$, which is almost exactly the same as that produced by the numerical model.

Figure 21 shows the spatial water surface profiles along the tank at different times throughout a sloshing wave cycle for the case $\omega/\omega_0 = 0{\cdot}999$. From the overall agreement with the linearized analytical model, it may be judged that the present scheme is suitable for

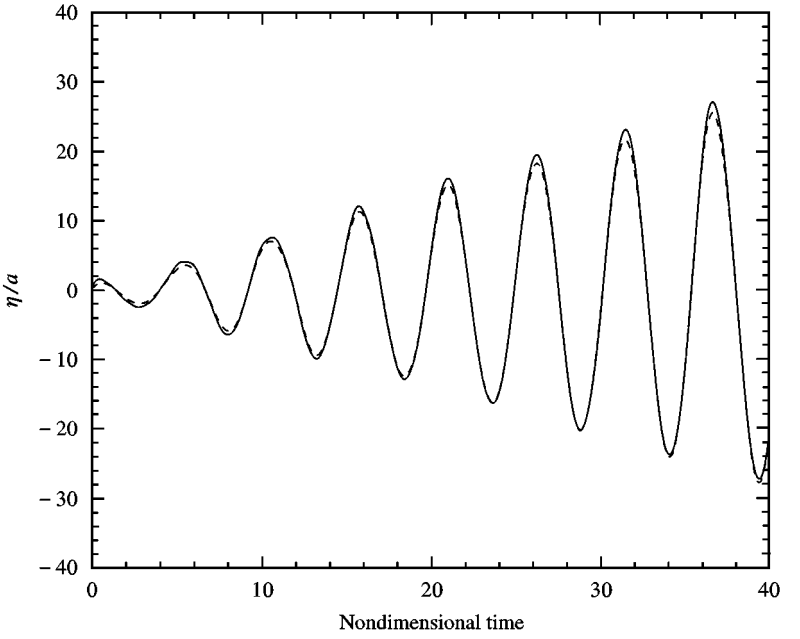

Figure 19. Time history at $x/d = -1$, $\omega/\omega_0 = 0{\cdot}999$: —, numerical result; - - -, linear solution.

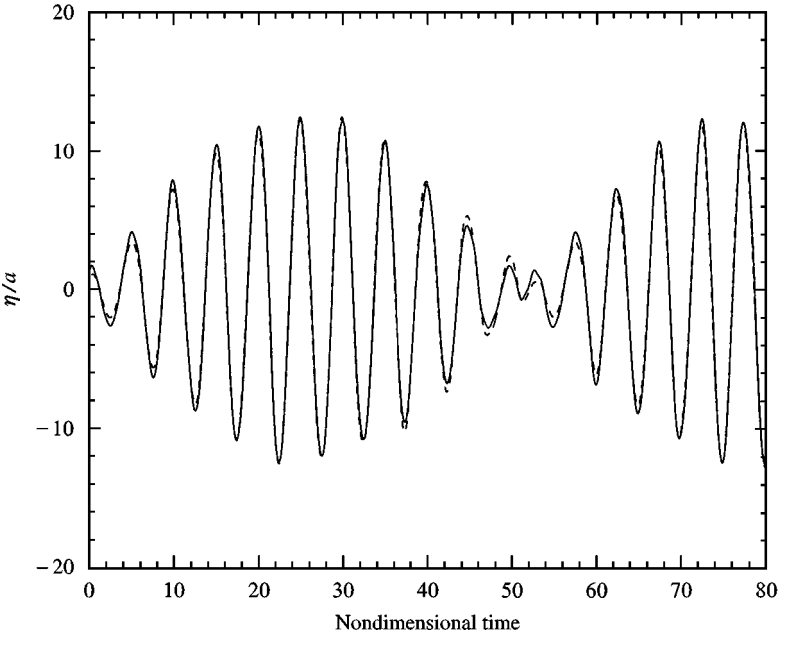

Figure 20. Time history at $x/d = -1$, $\omega/\omega_0 = 1{\cdot}1$: —, numerical result; - - -, linear solution.

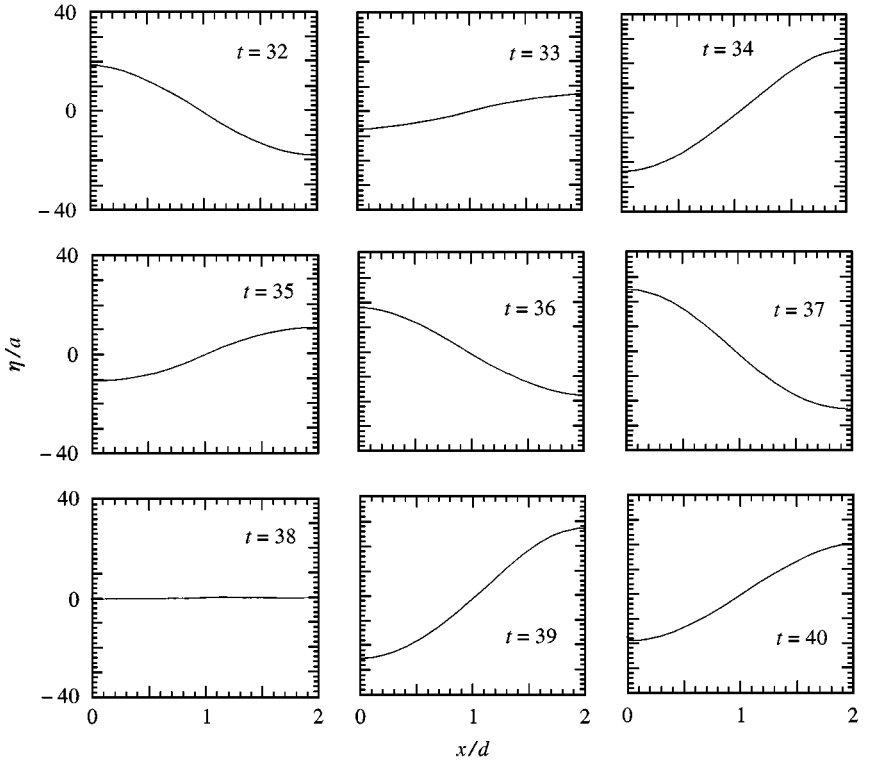

Figure 21. Wave profiles for the case $\omega/\omega_0 = 0{\cdot}999$ from $t = 32$ to 40.

predicting base-induced sloshing in tanks, provided the free-surface profile does not overturn.

6. CONCLUSIONS

The 2-D nonlinear time domain free-surface flow problem has been solved by the pseudospectral method. The σ-transformation eliminates any need for free-surface smoothing, unlike other approaches which do not use a mapped grid. Simulations have been obtained for standing waves in a fixed rectangular tank and for sloshing free-surface motions in a base-excited tank. From the standing-wave test cases, it is evident that the numerical method is very stable and requires fewer points in the discretization than other equivalent models [e.g., Wu & Eatock Taylor (1994)]. Grid-independent numerical results can be readily obtained. For transient free-surface waves of low steepness, almost exact agreement is obtained with analytical potential flow solutions up to second order. Nonlinear wave components above second order become increasingly evident in the solutions presented for wave steepnesses greater than $a/d = 0{\cdot}03$. The results for base-excited sloshing waves are very similar to linear analytical solutions derived by Wu *et al.* (1998); the larger wave motions are enhanced in the present numerical predictions due to nonlinear effects which are not included in the analytical model. Overall, it may be concluded that the present pseudospectral σ-transformed potential flow numerical scheme is useful for predicting nonoverturning free-surface wave motions. It should be straightforward to extend the present concepts to 3-D wave motions.

ACKNOWLEDGEMENTS

This research is supported by the Taiwan government, the British Overseas Research Student (ORS) Awards Scheme and a Wei-Lun Graduate Scholarship from St. Hugh's College, Oxford.

References

Abramson, H. N. 1966 The dynamic behaviour of liquid in moving containers. In Report SP 106 of NASA.

Basdevant, C., Deville, M., Haldenwang, P., Lacroix, J. M., Ouazzani, J., Peyret, R., Orlandi, P. & Patera, A. T. 1986 Spectral and finite difference solutions of the Burgers equation. *Computers and Fluids* **14,** 23–41.

Blumberg, G. L. & Mellor, G. L. 1980 A coastal ocean numerical model. In *Mathematical Modeling of Estuarine Physics* (eds J. Sundermann & K.P. Holz), pp. 203–219. Berlin:Springer

Cao, Y., Schultz, W. W. & Beck, R. F. 1991 Three dimensional desingularised boundary integral methods for potential problems. *International Journal for Numerical Methods in Fluids* **12,** 785–803.

Chen, W., Haroun, M. A. & Liu, F. 1996 Large amplitude liquid sloshing in seismically excited tanks. *Earthquake Engineering and Structural Dynamics* **25,** 653–669.

Cortes, A. B. & Miller, J. D. 1994 Solution of the Navier–Stokes equations by the spectral- difference method. *Numerical Methods for Partial Differential Equations* **10,** 345–368.

Craig, W. & Sulem, C. 1993 Numerical simulation of gravity waves. *Journal of Computational Physics* **108,** 73–83.

Dold, J. W. & Peregrine, D. H. 1986 An efficient boundary-integral method for steep unsteady water waves. In *Numerical Methods for Fluid Dynamics II* (eds K. W. Morton & M. J. Baines), pp. 671–679. Oxford:Oxford University Press.

Dommermuth, D. G., & Yue, D. K. P. 1987 A high-order spectral method for the study of nonlinear gravity waves. *Journal of Fluid Mechanics* **184,** 267–288.

Faltinsen, O. M. 1978 A numerical nonlinear method of sloshing in tanks with two-dimensional flow. *Journal of Ship Research* **22,** 193–202.

FENTON, J. D., & RIENECKER, M. M. 1982 A Fourier method for solving nonlinear water-wave problems: application to solitary-wave interactions. *Journal of Fluid Mechanics* **118,** 411-443.

GRILLI, S. T., SKOURUP, J. & SVENDSEN, I. A. 1989 An efficient boundary element method for non-linear water waves. *Engineering Analysis with Boundary Elements* **6,** 97–107.

HUSSAINI, M. Y. & ZANG, T. A. 1987 Spectral methods in fluid dynamics. *Annual Review of Fluid Mechanics* **19,** 339–367.

KU, H. C. & HATZIAVRAMIDIS, D. 1985 Solutions of the two-dimensional Navier-Stokes equations by Chebyshev expansion methods. *Computers and Fluids* **13,** 99–113.

KU, H. C., TAYLOR, T. D. & HIRSH, R. S. 1987a Pseudospectral methods for solution of the incompressible Navier–Stokes equations. *Computers and Fluids* **15,** 195–214.

KU, H. C., HIRSH, R. S. & TAYLOR, T. D. 1987b A pseudospectral method for solution of the three-dimensional incompressible Navier-Stokes equations. *Journal of Computational Physics* **70,** 439–462.

KU, H. C., HIRSH, R. S., TAYLOR, T. D. & Rosenberg, A. 1989 A pseudospectral matrix element method for solution of three-dimensional incompressible flows and its parallel implementation. *Journal of Computational Physics* **83,** 260–291.

LIN, W. N., NEWMAN, J. N. & YUE, D. K. 1984 Non-linear forced motions of floating bodies. *Proceedings of* 15*th Symposium on Naval Hydrodynamics*, The Hague, The Netherlands.

LONGUET-HIGGINS, M. S. & COKELET, E. D. 1976 The deformation of steep surface waves on water I. A numerical method of computation. *Proceedings of Royal Society* (*London*) (**A**)**350,** 1–26.

MELLOR, G. L. & BLUMBERG, A. F. 1985 Modeling vertical and horizontal diffusivities with the sigma coordinate system. *Monthly Weather Review* **113,** 1379–1383.

MITCHELL, A. R. & GRIFFITHS, D. F. 1980 *The Finite Difference Method in Partial Differential Equations* Chichester: Wiley.

PHILLIPS, N. A. 1957 A coordinate system having some special advantages for numerical forecasting. *Journal of Meteorology* **14,** 184–185.

STANSBY, P. K. & LLOYD P. M. 1995 A semi-implicit Lagrangian scheme for 3D shallow water flow with a two-layer turbulence model. *International Journal for Numerical Methods in Fluids* **20,** 115–133.

STREET, C. L., ZANG, T. A. & HUSSAINI, M. Y. 1985 Spectral multigrid methods with applications to transonic potential flow. *Journal of Computational Physics* **57,** 43–76.

TAYLOR, P. H. & VIJFVINKEL, E. 1998 Focussed wave groups on deep and shallow water. *Proceedings of the* 1998 *International OTRC Symposium*: *Ocean Wave Kinematics*, *Dynamics and Loads on Structures*, pp. 420–427. Houston, U.S.A.

TELSTE, J. G. 1985 Calculation of fluid motion resulting from large-amplitude forced heave motion of a two-dimensional cylinder in a free surface. *Proceedings* 4*th International Conference on Numerical Ship Hydrodynamics*, Washington, U.S.A.

TULIN, M. P., YAO, Y. & WANG, P. 1994 The simulation of the deformation and breaking of ocean waves in wave groups. In BOSS 94, 7*th International Conference on Behaviour of Offshore Structures*, (ed. C. Chryssostomidis),Vol. 2 pp. 383–392. New York: Elsevier Science Ltd.

WU, G. X. & EATOCK TAYLOR, R. 1994 Finite element analysis of two-dimensional non-linear transient water waves. *Applied Ocean Research* **16,** 363–372.

WU, G. X., MA, Q. W. & R. EATOCK TAYLOR 1998 Numerical simulation of sloshing waves in a 3D tank based on a finite element method. *Applied Ocean Research* **20,** 337–355.

ZHAO, R., & FALTINSEN, O. M. 1992 Water entry of two dimensional bodies. *Journal of Fluid Mechanics* **246,** 593–612.

APPENDIX: NOMENCLATURE

a	initial wave elevation amplitude
b	tank width
C_j, C_k	coefficients of formula used to evaluate Chebyshev parameters, $\hat{\mathbf{u}}$
d	still water depth
$\hat{\mathbf{G}}^{(q)}$	matrix to evaluate the qth derivative of a function
$\hat{\mathbf{G}}\mathbf{X}^{(q)}$	matrix to evaluate the qth derivative with respect to x
$\hat{\mathbf{G}}\mathbf{Y}^{(q)}$	matrix to evaluate the qth derivative with respect to y
g	acceleration due to gravity
h	local water depth, a function of distance, x, and time, t
N	number of collocation points

$\mathbf{T}$	matrix formed by Chebyshev polynomials
t	time
u	a one-dimensional function
$\hat{u}$	coefficient of Cheybshev expansion of u
x	horizontal coordinate in the physical domain
X	horizontal coordinate in the computational domain
y	vertical coordinate in the physical domain
Y	vertical coordinate in the computational domain
η	free-surface elevation above still water level
σ	sigma transformation variable which replaces y
ϕ	velocity potential function, $\phi(x,y,t)$
Φ	velocity potential function, $\Phi(x,\sigma,t)$